International Journal of Biomass & Renewables, 7(1) : 1 - 16, 2018

Influence of Volume Shrinkage and Water Evaporation on Heat Transfer and Chemical Reactions During the Pyrolysis of A Cellulose-Powder-Packed Bed

Ken-ichiro Tanoue[1*], Yuuki Hamaoka[1], Tatsuo Nishimura[1], Miki Taniguchi[2], Ken-ichi Sasauchi[2]

[1] Department of Mechanical Engineering, Yamaguchi University, Japan

[2] Chugai Ro Co., Ltd., Japan

Abstract

Heat and mass transfer during the pyrolysis of a cellulose-powder-packed bed has been investigated numerically to reveal volume shrinkage and water evaporation. From the calculation results for the temperature and velocity vector distributions, it was found that there is a quasi-steady state during pyrolysis because the gas volume increased on the top and side walls of the bed and then the effective thermal conductivity decreased. There were two plateaus in the time course of the temperature and two peaks in the time course of the generated gas flow rate for the experimental results. The calculated temperature with not only volume shrinkage but also additional water content reproduced the time course of the temperature after the second plateau. Furthermore, the calculation gas flow rate agreed quantitatively with the experimental ones, which had two peaks during pyrolysis. In order to reproduce the heat and mass transfer between the first and second plateaus in cellulose pyrolysis, it is necessary to investigate the modified calculation model with the heat of chemical reactions.

Keywords: Cellulose pyrolysis, temperature plateau, effective thermal conductivity, volume shrinkage, water evaporation

1 Introduction

There are two gasification methods for converting woody biomass: direct combustion and indirect gasification by external heating [1]. In the direct combustion method, attention has been paid to the downdraft gasifier because the gasifier has many merits, including its low price, the changeable facilities scale, and the ability to produce gas with a very low tar content [2-5]. The biomass was fed from the top of the downdraft gasifier while preheated air was fed from the side of the gasifier. The biomass packed bed in the gasifier was dried, pyrolyzed, deoxidized and finally divided into tar-free pyrolyzed gas and ash [2]. The role of the pyrolyzing zone is very important in these processes. In order to design a suitable downdraft gasifier with high efficiency, it is necessary to understand the heat and mass transfer during the pyrolysis of woody biomass.

There are many reports on heat transfer and heterogeneous chemical reactions during pyrolysis [6-12]. It has been reported that the volume of wood particles decreases during pyrolysis [13-15]. Davidsson, et al. [13] and Pattanotai, et al. [14] investigated the dependence on wood shrinkage in the longitudinal, tangential and radial directions against the annual rings of the wood. Their results [13, 14] showed that shrinkage along the longitudinal direction increased with char conversion and was higher than that in the radial direction. The dependence of the shrinkage on the direction was more remarkable at 30 K/s with larger particles because the char had large pores, which were greater than 45 μm [14]. Tanoue et al. [15] investigated the dependence of the shrinkage on the kinds of sawdust, with particles of less than 1 mm. Their results [15] shown that the volume of the packed bed for the stem of Pseudotsuga menziesii decreased by up to 60% of the original one after pyrolysis at 673 K. On the other hand, the volume for the bark of Pseudotsuga menziesii decreased up to only 80 % of the original one after pyrolysis at 673 K because the lignin content with a low pyrolysis rate in the bark was higher than that in the stem.

The influence of the shrinkage of a particle on heat and mass transfer have also been investigated using numerical simulations [16-22]. Di Blasi [16] derived the governing equations for heat and mass transfer taking into account the shrinkage during the pyrolysis of a particle. She defined three shrinkage factors (α, β and γ) to describe the volume of a particle. α shows the factor when the volume occupied by the solid is assumed to decrease with the char mass during devolatilization. β shows the factor of the volume left by the solid as a consequence of the devolatilization process. γ shows the ratio of the final gas volume to the initial one. By taking account of shrinkage ($\alpha = \gamma = 1, \beta = 0$), her calculation results for the time course of temperature distribution during pyrolysis of the particle agreed well with the experimental ones. Babu and Chaurasia [17] suggest that the calculation results with shrinkage ($\alpha = \gamma = 0.2, \beta = 0$) agree with a wide range of experimental results.

Although most researchers investigated using an isolated particle, a few reports have studied pyrolysis in a packed bed [23-27]. However, no report has investigated heat and mass transfer with shrinkage during pyrolysis in a packed bed.

In this paper, the governing equations for heat and mass transfer with shrinkage during pyrolysis in a packed bed have been

*Corresponding author.
E-mail address : tano@yamaguchi-u.ac.jp

expanded on the basis of the Blasi's shrinkage model [16] and Blasi and Russo's chemical reaction model [28] for an isolated wood sphere and derived. Furthermore, calculation results with not only shrinkage but also the evaporation of adsorbed water on the particle surface were compared with the experimental ones in a cellulose-powder-packed bed.

2 Numerical simulation

Numerical simulation during pyrolysis was conducted in a two-dimensional cylindrical coordinate. Figure 1 shows the calculation domain and boundary conditions in accordance with the experiment. The domain consisted of a packed bed and fire brick cell. Although the cell's name is "fire brick", it is vary porous material and its porosity is 0.7 [35]. So the inside of the cell was heated by the surrounded gas.

Figure 2 shows the reaction model during pyrolysis that was produced by Di Blasi and Russo [28]. In this paper, evaporation of absorbed water on the particle surface was also taken into account in the simulation.

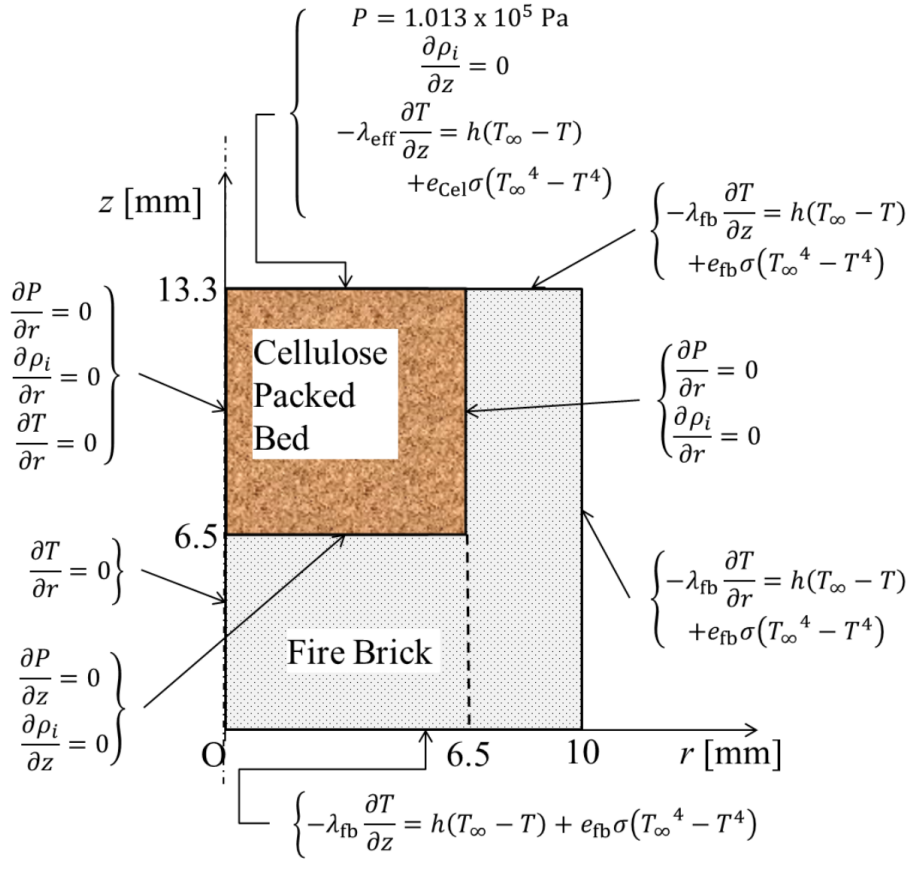

Figure 1 Two dimensional calculation domain and boundary conditions.

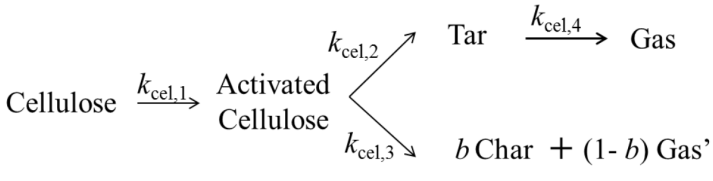

Figure 2 Chemical reaction model during pyrolysis [28].

Governing equations for mass transfer, motion of fluid flow and heat transfer during pyrolysis of biomass powder were derived as follows. Firstly, evaporation occurred and then the raw material changed to intermediate active solid. Secondly, the intermediate solid decomposed parallel to tar, gas and char. The material balance of these chemical reactions with the effect of volume shrinkage on the basis of ρ [kg/m^3] is written by the following equations.

$$\frac{d\rho_{\mathrm{H_2O\_liq}}}{dt} = -k_{0,\mathrm{Cel}}\ \rho_{\mathrm{H_2O\_liq}} - \frac{\rho_{\mathrm{H_2O\_liq}}}{V}\frac{dV}{dt} \tag{1}$$

$$\frac{d\rho_{\mathrm{Cel}}}{dt} = -k_{1,\mathrm{Cel}}\rho_{\mathrm{Cel}} - \frac{\rho_{\mathrm{Cel}}}{V}\frac{dV}{dt} \tag{2}$$

$$\frac{d\rho_{\mathrm{ias}}}{dt} = \left(k_{1,\mathrm{Cel}}\ \rho_{\mathrm{Cel}} - k_{2,\mathrm{Cel}}\ \ \rho_{\mathrm{ias}} - k_{3,\mathrm{Cel}}\ \rho_{\mathrm{ias}}\right) - \frac{\rho_{\mathrm{ias}}}{V}\frac{dV}{dt} \tag{3}$$

$$\frac{d\rho_{\mathrm{Char}}}{dt} = b\ \ k_{3,\mathrm{Cel}}\ \rho_{\mathrm{ias}} - \frac{\rho_{\mathrm{Char}}}{V}\frac{dV}{dt} \tag{4}$$

If the advection term due to pyrolysis is taken into account for gaseous products, the mass balances are given by,

$$\frac{\partial\varepsilon\rho_{\mathrm{H_2O\_Gas}}}{\partial t} + \frac{1}{r}\frac{\partial r\rho_{\mathrm{H_2O\_Gas}}U}{\partial r} + \frac{\partial\rho_{\mathrm{H_2O\_Gas}}W}{\partial z} = k_{0,\mathrm{Cel}}\ \rho_{\mathrm{H_2O\_liq}} - \frac{\varepsilon\rho_{\mathrm{H_2O\_Gas}}}{V}\frac{dV}{dt} \tag{5}$$

$$\frac{\partial\varepsilon\rho_{\mathrm{Tar}}}{\partial t} + \frac{1}{r}\frac{\partial r\rho_{\mathrm{Tar}}U}{\partial r} + \frac{\partial\rho_{\mathrm{Tar}}W}{\partial z} = k_{2,\mathrm{Cel}}\rho_{\mathrm{ias}} - \varepsilon k_{4,\mathrm{Cel}}\rho_{\mathrm{Tar}} - \frac{\varepsilon\rho_{\mathrm{Tar}}}{V}\frac{dV}{dt} \tag{6}$$

$$\frac{\partial\varepsilon\rho_{\mathrm{Gas}}}{\partial t} + \frac{1}{r}\frac{\partial r\rho_{\mathrm{Gas}}U}{\partial r} + \frac{\partial\rho_{\mathrm{Gas}}W}{\partial z} = (1-b)k_{3,\mathrm{Cel}}\rho_{\mathrm{ias}} + \varepsilon k_{4,\mathrm{Cel}}\rho_{\mathrm{Tar}} - \frac{\varepsilon\rho_{\mathrm{Gas}}}{V}\frac{dV}{dt} \tag{7}$$

Where *U* and *W* show volume averaged Darcy's velocities along the *r*-axis and the *z*–axis in the packed bed, respectively.

$$U = -\frac{\kappa}{\mu}\frac{\partial P}{\partial r} \tag{8}$$

$$W = -\frac{\kappa}{\mu}\frac{\partial P}{\partial z} \tag{9}$$

Where κ and μ show permeability in the packed bed and the viscosity of fluid, respectively.
The permeability is given by Kozeney Carman's empirical law [29],

$$\kappa = \frac{{D_p}^2}{150}\frac{\varepsilon^3}{(1-\varepsilon)^2} \tag{10}$$

Where D_p shows the particle size of the sample powder.
The material balance for the nitrogen gas is given by

$$\frac{\partial\varepsilon\rho_{\mathrm{N_2}}}{\partial t} + \frac{1}{r}\frac{\partial r\rho_{\mathrm{N_2}}U}{\partial r} + \frac{\partial\rho_{\mathrm{N_2}}W}{\partial z} = -\frac{\varepsilon\rho_{\mathrm{N_2}}}{V}\frac{dV}{dt} \tag{11}$$

The last terms of the right-hand sides in Equation (1-8) show the effect of volume shrinkage. The volume of an isolated particle with volume shrinkage is reported by Di Blasi [16] as follows.

$$V = V_S + V_{\mathrm{G}} \tag{12}$$

$$V_{\mathrm{S}} = V_{\mathrm{S0}}\left(\frac{G_{\mathrm{Cel}}}{G_{\mathrm{Cel,o}}} + \alpha\frac{G_{\mathrm{ias}}+G_{\mathrm{Char}}}{G_{\mathrm{Cel,o}}}\right) \tag{13}$$

$$V_{\mathrm{G}} = \beta(V_{\mathrm{S0}} - V_{\mathrm{S}}) + V_{\mathrm{G0}}\left(\frac{G_{\mathrm{Cel}}}{G_{\mathrm{Cel,o}}} + \gamma\left(1 - \frac{G_{\mathrm{Cel}}}{G_{\mathrm{Cel,o}}}\right)\right) \tag{14}$$

Where V_S and V_G show the solid volume and the gas one, respectively. α, β and γ show the shrinkage factor, the fraction of volume left by the solid during pyrolysis and the gas volume fraction of the initial one, respectively. If these shrinkage parameters are equal to 1, the volume does not change. Although Di Blasi made meaning to three volume shrinkage parameters [16], in fact, only the initial volume and volume after volume reduction could be measured. Therefore, we thought it appropriate to reduce the parameters. In this paper, these shrinkage parameters are assumed to be the same ones.

$$\alpha = \beta = \gamma = s \tag{15}$$

As for the validity of this assumption, we believe that it is necessary to conduct experiments in the future.
The porosity in the packed bed was defined by the following equation.

$$\varepsilon = \frac{V_{\mathrm{G}}}{V} \tag{16}$$

From the ideal gas law,

$$\frac{P}{\mathrm{R_G}T} = \frac{\rho_{\mathrm{Tar}}}{M_{\mathrm{Tar}}} + \frac{\rho_{\mathrm{Gas}}}{M_{\mathrm{Gas}}} + \frac{\rho_{\mathrm{H_2O\_Gas}}}{M_{\mathrm{H_2O}}} + \frac{\rho_{\mathrm{N_2}}}{M_{\mathrm{N_2}}} \tag{17}$$

Where R_G shows the universal gas constant.
The following pressure equation is obtained from Equations 5-8 and 16.

$$\frac{\partial\left(\varepsilon\frac{P}{T}\right)}{\partial t} - \frac{1}{r}\frac{\partial\left(r\frac{\kappa\partial PP}{\mu\partial rT}\right)}{\partial r} - \frac{\partial\left(\frac{\kappa\partial PP}{\mu\partial zT}\right)}{\partial z} = R_{\mathrm{G}}\left(\frac{k_{2,\mathrm{Cel}}\rho_{\mathrm{ias}} - \varepsilon k_{4,\mathrm{Cel}}\rho_{\mathrm{Tar}}}{M_{\mathrm{Tar}}} + \frac{bk_{3,\mathrm{Cel}}\rho_{\mathrm{ias}} + \varepsilon k_{4,\mathrm{Cel}}\rho_{\mathrm{Tar}}}{M_{\mathrm{Gas}}} + \frac{k_{0,\mathrm{Cel}}\ \rho_{\mathrm{H_2O\_liq}}}{M_{\mathrm{H_2O}}}\right) - \frac{\varepsilon P}{TV}\frac{dV}{dt} \tag{18}$$

The last term of the right-hand side in Equation 17 shows the effect of volume shrinkage. When a local thermodynamic equilibrium between gas and the solid phase components is assumed, the energy balance in the packed bed can be expressed by,

$$\frac{\partial\left[\left\{\varepsilon\left(\rho_{\mathrm{Tar}}C_{p,\mathrm{Tar}} + \rho_{\mathrm{Gas}}C_{p,\mathrm{Gas}} + \rho_{\mathrm{N_2}}C_{p,\mathrm{N_2}} + \rho_{\mathrm{H_2O_{Gas}}}C_{p,\mathrm{H_2O_{Gas}}}\right) + (1-\varepsilon)\left(\rho_{\mathrm{Cel}}C_{\mathrm{Cel}} + \rho_{\mathrm{ias}}C_{\mathrm{char}} + \rho_{\mathrm{Char}}C_{\mathrm{char}} + \rho_{\mathrm{H_2O_{liq}}}C_{p,\mathrm{H_2O_{liq}}}\right)\right\}T\right]}{\partial t} +$$

$$\frac{1}{r}\frac{\partial\left[\left(\rho_{\mathrm{Tar}}C_{p,\mathrm{Tar}} + \rho_{\mathrm{Gas}}C_{p,\mathrm{Gas}} + \rho_{\mathrm{N_2}}C_{p,\mathrm{N_2}} + \rho_{\mathrm{H_2O_{Gas}}}C_{p,\mathrm{H_2O_{Gas}}}\right)rUT\right]}{\partial r} + \frac{\partial\left[\left(\rho_{\mathrm{Tar}}C_{p,\mathrm{Tar}} + \rho_{\mathrm{Gas}}C_{p,\mathrm{Gas}} + \rho_{\mathrm{N_2}}C_{p,\mathrm{N_2}} + \rho_{\mathrm{H_2O_{Gas}}}C_{p,\mathrm{H_2O_{Gas}}}\right)WT\right]}{\partial z} =$$

$$\frac{V_0}{V}\left\{\frac{1}{r}\frac{\partial}{\partial r}\left(r\lambda_{eff}\frac{\partial T}{\partial r}\right) + \frac{\partial}{\partial z}\left(\lambda_{eff}\frac{\partial T}{\partial z}\right)\right\} +$$

$$\frac{\left[\left\{\varepsilon\left(\rho_{\mathrm{Tar}}C_{p,\mathrm{Tar}} + \rho_{\mathrm{Gas}}C_{p,\mathrm{Gas}} + \rho_{\mathrm{N_2}}C_{p,\mathrm{N_2}}\right) + (1-\varepsilon)\left(\rho_{\mathrm{Cel}}C_{\mathrm{Cel}} + \rho_{\mathrm{ias}}C_{\mathrm{char}} + \rho_{\mathrm{Char}}C_{\mathrm{char}}\right)\right\}(T-T_0)\right]}{V}\left(-\frac{dV}{dt}\right) + \left(-\Delta H_{\mathrm{H_2O}}\right)\left(k_{0,\mathrm{Cel}}\ \rho_{\mathrm{H_2O\_liq}}\right) \tag{19}$$

Where V_0 shows the initial volume before the pyrolysis. The effective thermal conductivity was calculated by using Kunii's formula [30].

$$\lambda_{\mathrm{eff}} = \lambda_{\mathrm{v}} \left\{ \varepsilon \left(1 + \frac{a_1 D_p}{\lambda_{\mathrm{v}}} \right) + \frac{(1-\varepsilon)}{\left(\frac{1}{\frac{1}{\phi} + \frac{\lambda_{\mathrm{v}}}{a_2 D_{\mathrm{p}}}} + \frac{2\lambda_{\mathrm{v}}}{3\lambda_{\mathrm{s}}} \right)} \right\} \tag{20}$$

$$a_1 = 0.1952 \frac{e_{\mathrm{Cel}}}{1-e_{\mathrm{Cel}}} \left(\frac{T}{100} \right)^3 \tag{21}$$

$$a_2 = \frac{0.1952}{1+\frac{\varepsilon}{1-\varepsilon}\frac{1-e_{\mathrm{Cel}}}{e_{\mathrm{Cel}}}} \frac{e_{\mathrm{Cel}}}{1-e_{\mathrm{Cel}}} \left(\frac{T}{100} \right)^3 \tag{22}$$

Where λ_s and λ_v show the solid and volatile thermal conductivities, respectively. The λ_s was calculated by taking account of varying from virgin wood to char [16].

$$\lambda_{\mathrm{S}} = \lambda_{\mathrm{Cel}} \left(1 - \frac{G_{\mathrm{ias}} + G_{\mathrm{Char}}}{G_{\mathrm{Cel,0}}} \right) + \lambda_{\mathrm{Char}} \left(\frac{G_{\mathrm{ias}} + G_{\mathrm{Char}}}{G_{\mathrm{Cel,0}}} \right) \tag{23}$$

On the other hand, the λ_v was assumed to be the thermal conductivity of nitrogen gas. The third term on the right-hand side in Eq. (18) shows the effect of volume shrinkage. In order to investigate the dependence of the volume shrinkage on the time course of temperature during pyrolysis, the heat of reaction except for the evaporation of water is assumed to be 0 J/kg. The latent heat of water is shown in [31]. For fire brick cell, the energy balance is written by,

$$\rho_{\mathrm{fb}} C_{\mathrm{fb}} \frac{d\ T}{dt} = \frac{1}{r}\frac{\partial}{\partial r}\left(r\lambda_{\mathrm{fb}} \frac{\partial T}{\partial r} \right) + \frac{\partial}{\partial z}\left(\lambda_{\mathrm{fb}} \frac{\partial T}{\partial z} \right) \tag{24}$$

To solve heat and mass transfer during the pyrolysis of a 0.5 g biomass input, these governing equations and the boundary conditions are discretized over a control volume using the finite difference method. The local volume shrinkage effect of heat transfers during pyrolysis at (i, j) is given by,

$$q_{\mathrm{VS},i,j} = \frac{\left\{ \left[\left((1-\varepsilon)\left(\rho_{\mathrm{Cel}} C_{\mathrm{Cel}} + \rho_{\mathrm{ias}} C_{\mathrm{char}} + \rho_{\mathrm{Char}} C_{\mathrm{char}} + \rho_{\mathrm{H_2O_{liq}}} C_{p,\mathrm{H_2O_{liq}}} \right) + \varepsilon\left(\rho_{\mathrm{Tar}} C_{p,\mathrm{Tar}} + \rho_{\mathrm{Gas}} C_{p,\mathrm{Gas}} + \rho_{\mathrm{N_2}} C_{p,\mathrm{N_2}} + \rho_{\mathrm{H_2O_{Gas}}} C_{p,\mathrm{H_2O_{Gas}}} \right) \right) \right] (T - T_0) \right\}}{V} \left(-\frac{dV}{dt} \right) \Bigg|_{i,j} r_i \Delta r_i \Delta z_j \tag{25}$$

In considering the interaction between the local position (i, j) and the surrounding ones ((i+1,j), (i-1,j), (i, j+1) and (i,j-1)), the average heat transfer rate due to the volume shrinkage is assumed by,

$$Q_{\mathrm{VS},i,j} = \frac{1}{4}\left\{ \left(q_{\mathrm{VS},i,j} - q_{\mathrm{VS},i+1,j} \right) + \left(q_{\mathrm{VS},i,j} - q_{\mathrm{VS},i-1,j} \right) + \left(q_{\mathrm{VS},i,j} - q_{\mathrm{VS},i,j+1} \right) + \left(q_{\mathrm{VS},i,j} - q_{\mathrm{VS},i,j-1} \right) \right\} \tag{26}$$

Average mass transfer rates due to volume shrinkage are also discretized in the same way.

Temperature and pressure are solved by the SOR method while the densities of components are solved by the 4th order Runge Kutta method.

The dependence of all physical properties on the temperature is described in Table 1.The kinetic parameters in the equations by Di Blasi C and Russo G [28] are listed in Table 2.

Table 1 Physical properties

	Nomenclature			Equation	Reference
Specific heat [J/kg/K]	*C* (Solid)	Packed bed	Cellulose	**-213+4.85 *T***	9, 32
			Activated Cellulose	**432+2.09 *T***	Present work
			Char	**432+2.09 *T***	9, 33
	Cp (Gas)		Tar	**-100+4.4 T-0.00157 T^2**	34
			Gas	**770+0.629 T-0.000191 T^2**	34
			Nitrogen	**975+0.187 T-1.43×10^{-7} T^2**	Present work
		Fire brick		1004.652	35
Thermal conductivity [W/m/K]	λ	Packed bed	Cellulose	(0.1046+0.255+0.255)/3	36
			Activated Celulose	(0.071+0.105+0.105)/3	Present work
			Char	(0.071+0.105+0.105)/3	36
			Tar, Gas, Nitrogen and Volatile	**0.000331$T^{0.763}$**	Present work
		Fire brick		**0.39**	35
Initial density of Cellulose packed bed [kg/m^3]	$\rho_{Cel,0}$	Packed bed		554	Present work
Density of fire brick [kg/m^3]	r_{fb}	Fire brick		780	35
Emissivity [-]	*e*	Packed bed		0.95	9
		Fire brick		0.80	35
Cellulose particle size [mm]	*D*p	Packed bed		27.3	Present work
Viscosity [Pa s]	μ	Packed bed (Nitrogen)		4.55 x 10^{-7} $T^{0.653}$	Present work

Table 2 Kinetic parameters in Blasi and Russo's chemical reaction model [28].

Parameters	
$k_{Cel,i}$ [1/s] (Unit of activation energy [J/mol])	$k_{Cel,1} = 2.80 \times 10^{19} e^{-\frac{186700}{R_G T}}$
	$k_{Cel,2} = 3.28 \times 10^{14} e^{-\frac{196500}{R_G T}}$
	$k_{Cel,3} = 1.30 \times 10^{10} e^{-\frac{150500}{R_G T}}$
	$k_{Cel,4} = 4.28 \times 10^{6} e^{-\frac{108000}{R_G T}}$
b	0.35

3 Experimental

Cellulose powder of 0.5 g was packed into a cylindrical fire brick cell (Isolite Insulating Products Co., Ltd.), which had an inner volume of about 1 cc. The cellulose powder was made of Sigma-Aldrich and its average particle size was 27.3 μm. A bared K-type thermocouple was used to measure the temperature at the center in the packed bed during pyrolysis. The diameter of the thermocouple was 100 μm. The thermocouple was shielded by alumina tube. The alumina tube and the cylindrical cell were connected by stainless wires.

The experimental apparatus consisted of a nitrogen gas supply, a tubular reactor, cold traps for tar and water, and a gas flow meter. The diameter and the height of the tubular reactor were 106 mm and 230 mm, respectively. The furnace had a maximum output of 1.5 kW, and the temperature at the wall of the tubular reactor could be set at the setting temperature, T_S. The T_S was 673 K. The cold traps, which were situated in an ice bath, were two 500-mL Erlenmeyer flasks filled with glass wool and solid $CaCl_2$. During the pyrolysis, tar and water were adsorbed by the traps, and gas was generated in the reaction that flowed through the traps. The gas flow rate was measured using a wet-type gas meter (Shinagawa Co., Ltd., W-NK-2B). Before the experiment, air in the reactor was replaced by nitrogen gas. Fast pyrolysis was started by entering the cylindrical cell having the thermocouple into the tubular reactor. The generated gas flow rate and the temperature at the center of the cell were measured simultaneously during pyrolysis up to 10 min.

4 Evaporation rate constant

A thermogravimetric experiment was conducted to investigate the evaporation rate constant $k_{0,Cel}$. The initial mass was a few tens of mg. In order to estimate the mass of the water content absorbed on the particle surface as accurately as possible, the temperature was kept at about 373 K during 120 min after the temperature approached about 373 K.

5 Results and Discussion

5.1 Grid sensitivity

Figure 3 shows the calculation results of grid dependence for the time course of the temperature at the center in the packed bed and generated gas flow rate from the top surface of the packed bed during the pyrolysis of cellulose powder. The results did not change for the temperature and the gas flow rate when the set of grid numbers was greater than (N_r , N_z) = (40, 48). In this paper, (N_r , N_z) = (40, 48) was selected as the set of grid numbers.

5.2 Time course of temperature and velocity distributions during pyrolysis

Figure 4 shows the calculation result for no shrinkage case in the time course of the temperature and velocity vector distributions in the packed bed during cellulose pyrolysis. At t = 50 s, the heat transfer could be controlled by thermal conduction because there were no velocity vectors. On the other hand, at t > 200 s, as cellulose decomposition would occur, the heat transfers in the bed depended on not only thermal conduction but also advection due to pyrolysis. In particular, the temperature and velocity vector distributions were almost the same from t = 200 s to t = 300 s. In order to determine the reason for this, the porosity and the effective thermal conductivity distributions at t = 200 s were investigated as shown in Figure 5. When the pyrolysis occurred in the bed, porosity on not only the top surface of the packed bed but also the side wall of the fire brick cell was close to 1. In other words, the gas volume increased near the side wall and the adiabatic effect occurred. The effective thermal conductivity became smaller at regions other than that at the central region of the packed bed. Then advection terms and heat conduction terms in eq. 19 could be balanced. So, the temperature and velocity vector distributions were almost the same from t = 200 s to t = 300 s as shown in Figure 4.

5.2 Influence of volume shrinkage on heat and chemical reactions during pyrolysis

Figure 6 shows the calculation results of the volume shrinkage effect in a packed bed for the time course of the temperature at the center in the packed bed and generated gas flow rate from the top surface of the packed bed during the pyrolysis of cellulose powder. If there was no volume shrinkage, the temperature increased monotonously over time and gas was generated at 1.2 min. As time elapsed, the temperature had an almost constant due to not only the decrement of the effective thermal conductivity at the side wall of the fire brick cell but also the balance between the advection term and thermal conduction term in Equation 19. The generation gas flow rate reached maximum at about 3 min when the temperature had an almost constant. After that the gas flow rate decreased with time. When the volume shrinkage was taken into consideration at s = 0.8, the temperature at t > 2min was slightly higher than that of no shrinkage case. The maximum gas flow rate was also slightly higher than that of no shrinkage case. The lower the shrinkage factor, these tendencies were more remarkable. Especially, s < 0.4, when the gas generation approached to 0 L/min, the temperature increased again due to thermal conduction and finally had a constant temperature of an environmental one at 673 K.

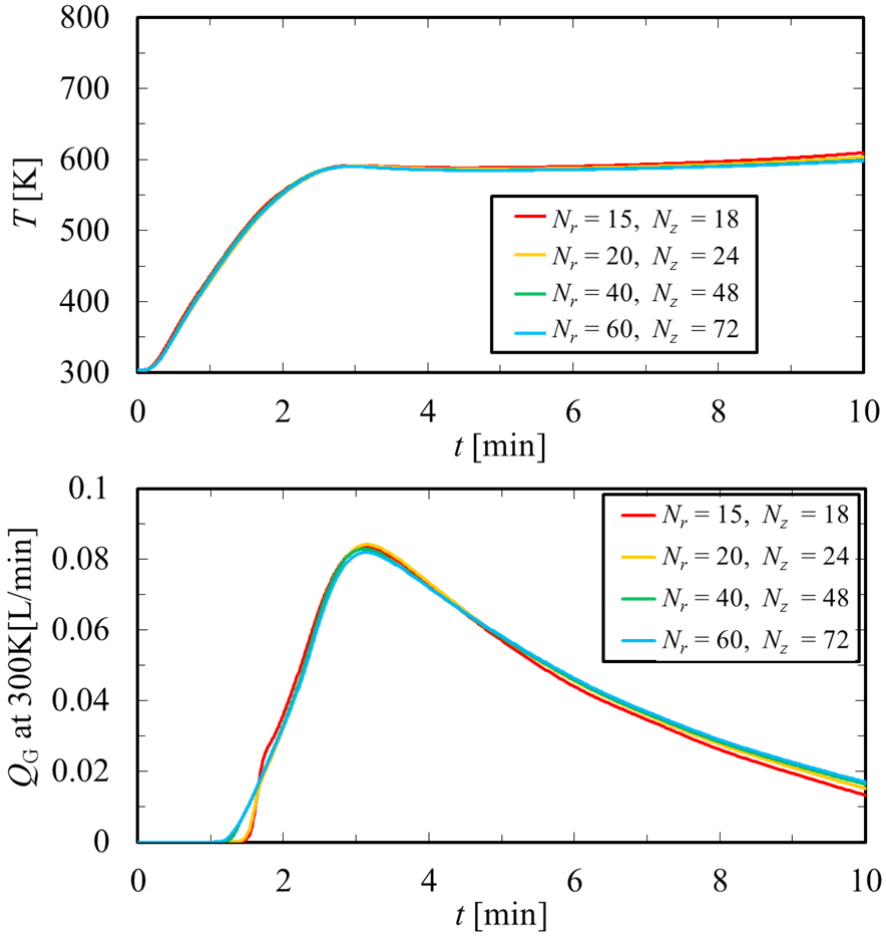

Figure 3 Calculation results of grid dependence for time course of a) temperature at the center inthe packed bed and b) generated gas flow rate from the top surface of the packed bed during pyrolysis of cellulose powder.

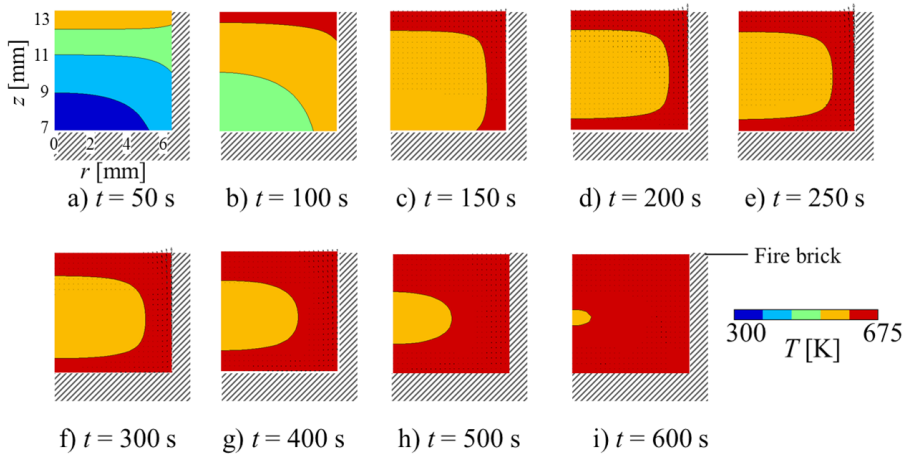

Figure 4 Time course of temperature and velocity vectors distribution in the cellulose packed bed.

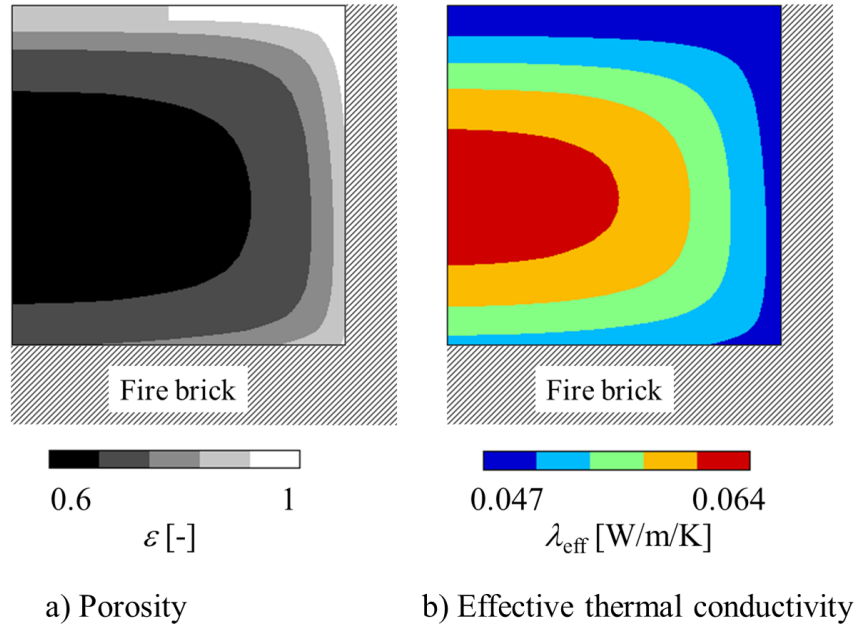

Figure 5 Porosity and Effective thermal conductivity distribution in the cellulose packed bed at t = 200 s.

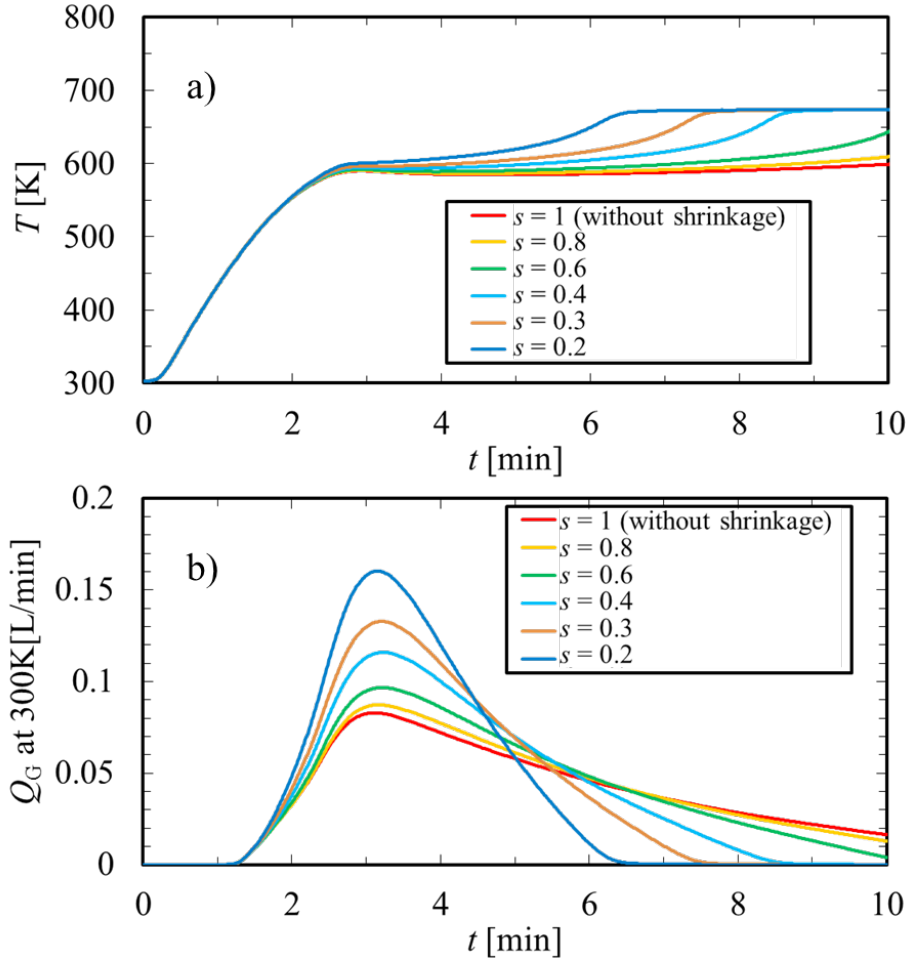

Figure 6 Dependence of heat and mass transfer during pyrolysis in the cellulose packed bed on the shrinkage parameter s.

5.3 Influence of evaporation on heat and chemical reactions during pyrolysis

Figure 7 shows the time courses of the mass of residue and temperature during evaporation of water from cellulose powder using thermogravimetry. The mass decreased over time and approached a constant value at about 373 K. Therefore, the decrement mass could be regarded as water absorbed on the surface of the cellulose powder. If the evaporation rate is assumed to depend on the first order of the mass of water

Figure 8 shows Arrhenius plots of the evaporation rate constant for cellulose powder. The dispersions of the data at relatively high and low temperatures are large. Immediately after the start of heating at 300 K < T < 320 K, there is a temperature distribution inside the container of TG, so it is conceivable that the evaporation rate includes a large variation. On the other hand, as the moisture was depleted near the boiling point at 373 K, the evaporation rate could become small, and its fluctuation amount also could increase. From the Arrhenius plots, the evaporation rate constant can be expressed by,

$$\frac{dG_{\mathrm{H_2O\_liq}}}{dt} = -k_{0,\mathrm{Cel}} \quad G_{\mathrm{H_2O\_liq},i} \tag{27}$$

$$\therefore \quad k_{0,\mathrm{Cel}} \quad = -\frac{1}{G_{\mathrm{H_2O\_liq}}} \frac{dG_{\mathrm{H_2O\_liq}}}{dt} \tag{28}$$

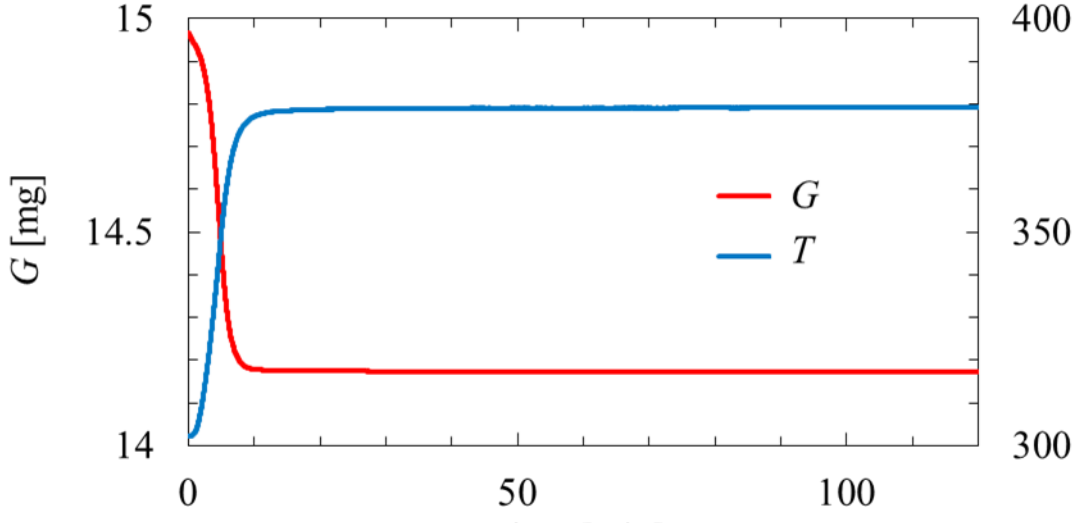

Figure 7 Time courses of mass of residue and temperature during evaporation of water from cellulose powder using the thermogravimetry.

$$k_{0,\mathrm{Cel}} = k_{\mathrm{f0,Cel}} \exp\left(-\frac{\Delta E}{\mathrm{R_G}T}\right). \tag{29}$$

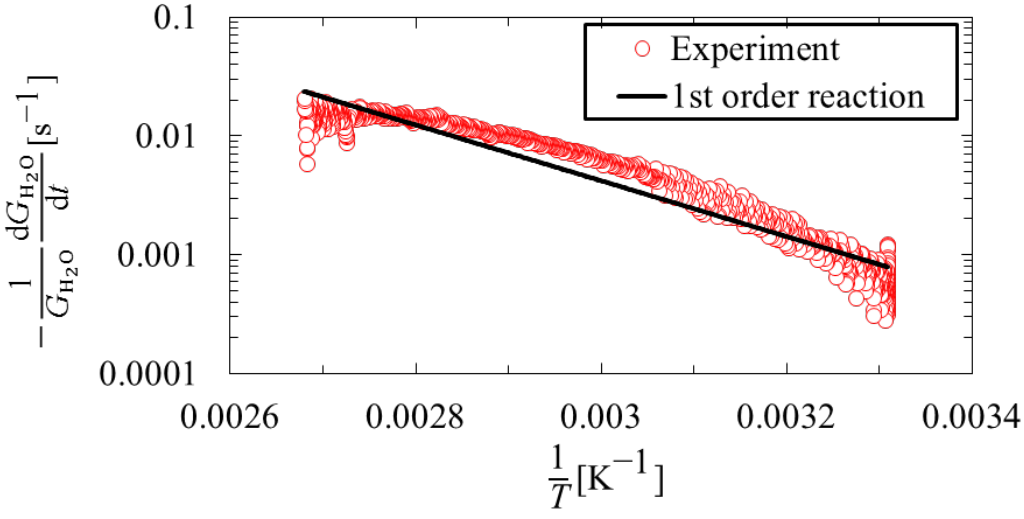

Figure 8 Arrhenius plot of water vaporization from the cellulose powder.

Where $k_{\mathrm{f0,Cel}}$ and ΔE for cellulose powder were 46,100 s^{-1} and 44,900 J/kg, respectively.
The mass fraction of the additional water content is given by

$$w_{\mathrm{H_2O}} = \frac{G_{\mathrm{H_2O,0}}}{G_{\mathrm{Cel,0}}} \tag{30}$$

Where shows the initial mass of additional water. For the cellulose powder, the initial mass of additional water was about 0.05 in the thermogravimetric experiment. The initial density of the additional water is given by

$$\rho_{\mathrm{H_2O_{liq,0}}} = \frac{G_{\mathrm{H_2O,0}}}{V_0} \tag{31}$$

A calculation with the effect of additional water content was carried out by changing the initial density of the additional water. Fig. 9 shows the calculation results of the effect of additional water content in the packed bed for the time course of the temperature at the center in the packed bed and generated gas flow rate from the top surface of the packed bed during the pyrolysis of cellulose powder. The shrinkage factor was equal to 0.3. If the water absorbed to the cellulose surface, there was an infection point at 373 K of the temperature and the vapor generated. The more the additional water, the more remarkable the infection point and the more the vapor.

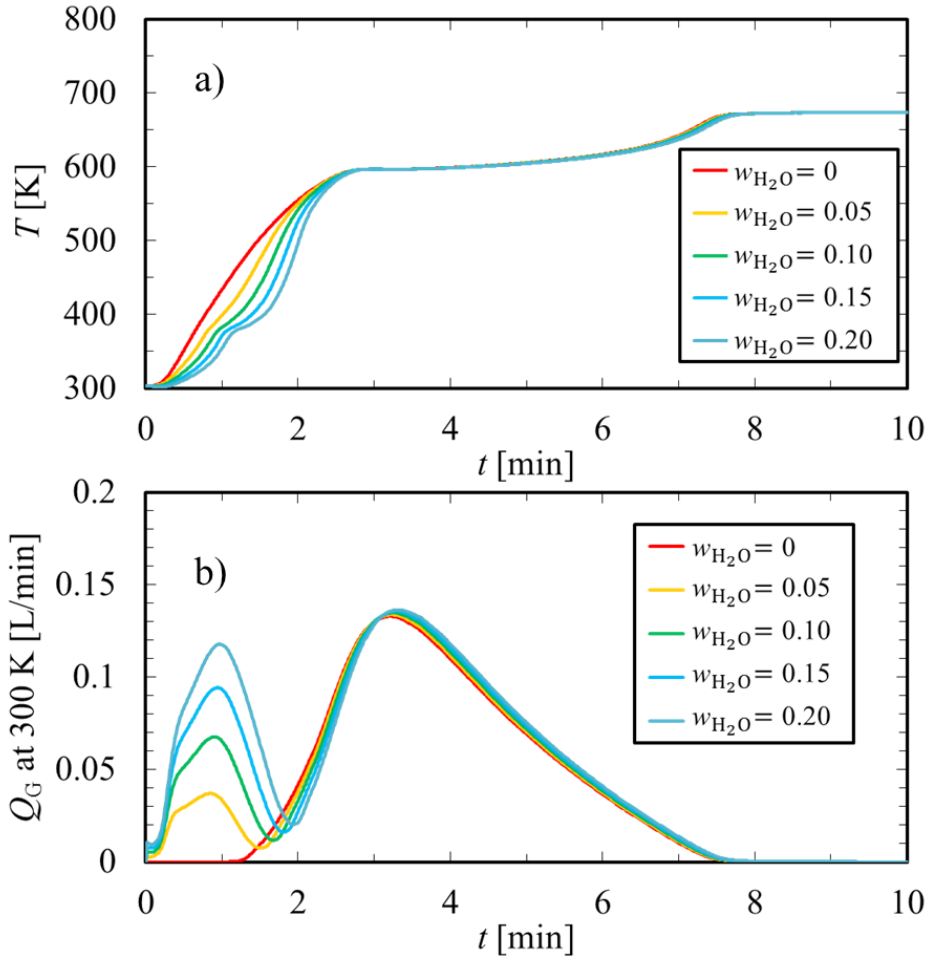

Figure 9 Dependence of heat and mass transfer during cellulose powder pyrolysis in the packed bed on the water content.

5.5 Comparison of calculation results with experimental ones

Figure 10 shows the time course of temperature in a packed bed and the generated gas flow rate during cellulose powder pyrolysis. The plots and lines show the experimental and calculation results, respectively. There were two plateaus in the time course of temperature for the experimental results. The calculation results without both volume shrinkage and additional water content did not agree with the experimental ones for temperature and the gas flow rate. On the other hand, the calculation temperature with volume shrinkage (s = 0.3) agreed well with the experimental one after the second plateau. In this study, we considered s = 0.3 to be close to the tendency of temperature change of the experimental value. However, in reality, it is necessary to evaluate the volume shrinkage parameter using various particles in the future work. Furthermore, the calculation gas flow rate with water additional content () agreed well with the experimental one at t < 1 min. However, the experimental results could not be reproduced by the calculation results with both volume shrinkage and additional water content at 1 min < t < 4 min because of not taking into account the heat of the chemical reactions in this study.

In a future study, the heat of reactions due to the decomposition of cellulose will be measured by differential scanning calorimetry and the results examined using the modified calculation model.

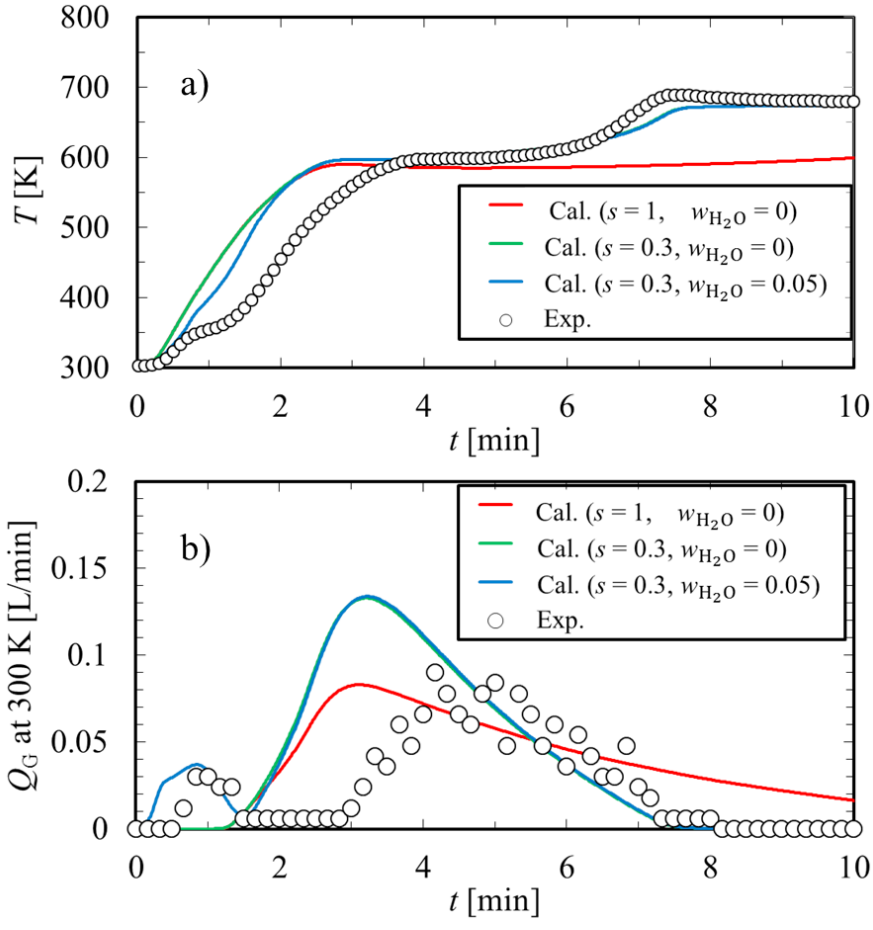

Figure 10 Comparison of calculation results of heat and mass transfer during cellulose powder pyrolysis in the packed bed with experimental ones.

6 Conclusion

Heat and mass transfer during the pyrolysis of a cellulose-powder-packed bed were investigated numerically to focus on the volume of shrinkage. The following conclusions were obtained:

1) From the calculation results on the temperature and velocity vector distributions, it was found that there was a quasi-steady state during pyrolysis because the gas volume increased on the top and side walls of the bed and effective thermal conductivity decreased.

2) There were two plateaus in the time course of temperature and two peaks in the time course of the generated gas flow rate for the experimental results. The calculation temperature with not only volume shrinkage but also additional water content reproduced the time course of temperature after the second plateau. Furthermore, the calculation gas flow rate agreed quantitatively with the experimental ones, which had two peaks during pyrolysis.

3) In order to reproduce heat and mass transfer between the first and second plateau in cellulose pyrolysis, it is necessary to investigate the modified calculation model with the heat of chemical reactions.

Acknowledgement

This work was supported in part by a Grant-in Aid for Scientific Research C (No. 17K06196) from the Japan Society for the Promotion of Science.

Nomenclature

a_1	Defined in Eq. 21	[W/(m^{2}K)]
a_2	Defined in Eq. 22	[W/(m^{2}K)]
b	kinetic parameter in in Blasi and Russo's chemical reaction model [28]	[-]
C	Specific heat of solid component	[J/(kg K)]
Cp	Specific heat of gaseous component at constant pressure	[J/(kg K)]
D_p	Particle size of Cellulose powder	[m]
e	Emissivity	[−]
ΔE	Activation energy of evaporation	[J/mol]
G	Mass	[kg]
h	Heat transfer coefficient between biomass and gas	[W/(m^{2}K)]
ΔH_{H_2O}	Latent heat of water evaporation	[J/kg]
i	Grid number along r direction in the packed bed	[-]
j	Grid number along z direction in the packed bed	[-]
$k_{n,\mathrm{Cel}}$	Reaction rate constant of component n in Cellulose powder	[1/s]
$k_{\mathrm{f0,Cel}}$	Frequency factor of water evaporation	[1/s]
M_n	Molecular weight of component n	[kg/mol]
N	Maximum grid number	[-]
P	Pressure	[Pa]
Q_{VS}	Average heat transfer rate due to the volume shrinkage	[-]
Q_{G}	Gas flow rate	[L/min]
$q_{\mathrm{VS},i,j}$	Local volume shrinkage effect of heat transfer during pyrolysis at (i, j)	[-]
$\mathrm{R_G}$	Universal gas constant （= 8.314 J/(mol K)）	[J/(mol K)]
r	r component in the packed bed	[-]
Δr_i	grid size i along r direction in the packed bed	[m]
s	Volume shrinkage parameter in Eq. 15	[-]
T	Temperature	[K]
t	Operation time	[s]
U	Volume averaged Darcy's velocity along the r–axis in the packed bed	[m/s]
V	Volume	[m^3]
W	Volume averaged Darcy's velocity along the z–axis in the packed bed	[m/s]
w	Mass fraction	[-]
z	z component in the packed bed	[-]
Δz_j	grid size j along z direction in the packed bed	[m]

Greek symbol

α	Volume shrinkage parameter in Eq. 13	[-]
β	Volume shrinkage parameter in Eq. 14	[-]
γ	Volume shrinkage parameter in Eq. 14	[-]
ε	Porosity in Eq. 16	[-]
ø	(Effective thickness of fluid film)/D_p in Ref. 30	[-]
κ	Permeability	[m^2]
λ	Thermal conductivity	[W/(mK)]
μ	Viscosity	[Pa s]
ρ	Density	[kg/m^3]
σ	Stefan-Boltzman constant (=5.669x10^{-8} W/m^{2}K^4)	[W/m^{2}K^4]

Subscript	
Cel	Cellulose powder
Char	Char
eff	effective
fb	Fire brick
Gas	Gas
H_2O_liq	Water in liquid phase
H_2O_Gas	Water in gas phase
ias	Intermediate activated solid
N_2	Nitrogen
r	*r* component
S	solid
Tar	Tar
v	volatile
z	*z* component
0	Initial value
∞	Environmental condition near the fire brick

References

[1] S. Heyne, H. Thunman, S. Harvey, Exergy-based comparison of indirect and direct biomass gasification technologies within the framework of bio-SNG production, *Biomass Conv Bioref*, 3, pp. 337–52, 2013.

[2] A. Bhavanam, R.C. Sastry, Biomass gasification processes in downdraft fixed bed reactors: A Review, *Int J Chem Eng Appl*, 2(6), pp. 425-33, 2011.

[3] T.K. Patra, P.N. Sheth, Biomass gasification models for downdraft gasifier: A state-of-the-art review, *Renew Sustain Energy Rev*, 50, pp. 583–93, 2015.

[4] N.A. Inglea, S.S. Lakadeb, Design and development of downdraft gasifier to generate producer gas, *Energy Procedia*, 90, pp. 423 – 31, 2016.

[5] P.N. Sheth, B.V. Babu, Experimental studies on producer gas generation from wood waste in a downdraft biomass gasifier, *Biores Technol*, 100, pp. 3127–33, 2009.

[6] C. Di Blasi, Modeling chemical and physical processes of wood and biomass pyrolysis, *Prog Energy Combust Sc*i, 34, pp. 47-90, 2008.

[7] N. Prakash, T. Karunanithi, Advances in modeling and simulation of biomass pyrolysis, *Asian J Sci Res,* 2(1), pp. 1-27, 2009.

[8] D.L. Pyle, C.A. Zaror, Heat transfer and kinetics in the low temperature pyrolysis of solids, *Chem Eng Sci*, 39, pp. 147-58, 1984.

[9] C.A. Koufopanpos, N. Papayannakos, G. Maschio and A. Lucchesi, Modeling of the pyrolysis of biomass particles. Studies on kinetics, thermal and heat transfer effects, *Can J Chem Eng*, 69, pp. 907-15,1991.

[10] R.S. Miller, J. Bellan, A generalized biomass pyrolysis model based on superimposed cellulose, hemicellulose and lignin kinetics, *Combust Sci Technol*, 126, pp. 97-137, 1997.

[11] W.C. Park, A. Atreya, H.R. Baum, Experimental and theoretical investigation of heat and mass transfer processes during wood pyrolysis, *Combust Flame*, 157, pp. 481-94, 2010.

[12] P.O. Okekunke, T. Pattanotai, H. Watanabe, K. Okazaki, Numerical and experimental investigation of intra-particle heat transfer and tar decomposition during pyrolysis of wood biomass, *J Therm Sci Technol*, 6(3), pp. 360-75, 2011.

[13] K.O. Davidsson, J.B.C. Pettersson, Birch wood particle shrinkage during rapid pyrolysis, *Fuel*, 81, pp. 263-70, 2002.

[14] T. Pattanotai, H. Watanabe, K.Okazaki, Gasification characteristic of large wood chars with anisotropic structure, *Fuel*, 150, pp. 331-39, 2014.

[15] K. Tanoue, K. Yamasaki, T. Nishimura, M. Taniguchi, K. Sasauchi, A relationship between the formation rate of solid component and volume reduction of packed bed of woody biomass particles during pyrolysis, *J Japan Inst Energy*, 90; pp. 1031-372011 (in Japanese).

[16] C. Di Brasi. Heat, momentum and mass transport through a shrinking biomass particle exposed to thermal radiation, *Chem Eng Sci*, 51(7), pp.1121-32, 1996.

[17] B.V. Babu and A.S. Chaurasia, Heat transfer and kinetics in the pyrolysis of shrinking biomass particle, *Chem Eng Sci*, 59, pp. 1999-2012, 2004.

[18] M. Bellais, K.O. Davidsson, T. Liliedahl, K. Sjostrom, J.B.C. Pettersson, Pyrolysis of large wood particles: a study of shrinkage importance in simulation, *Fuel*, 82, pp. 1541-48, 2003.

[19] M.J. Hagge, K.M. Bryden, Modeling the impact of shrinkage on the pyrolysis of dry biomass, Chem Eng Sci, 57, pp. 2811-23, 2002.

[20] K.M. Bryden, M.J. Hagge, Modeling the combined impact of moisture and char shrinkage on the pyrolysis of a biomass particle, *Fuel*, 82, pp. 1633-44, 2003.

[21] Shi Xi, F. Ronsse, J.G. Pieters, Finite element modeling of intraparticle heterogeneous tar conversion during pyrolysis of woody biomass particles, *Fuel Proc Technol*, 148, pp. 302-16, 2016.

[22] H. Zhong, J. Zhang, Y. Zhu, S. Liang, Multi-fluid modeling biomass fast pyrolysis in the fluidized-bed reactor including particle shrinkage effects, *Energy Fuels*, 30, pp. 6440-47, 2016.

[23] M. Fatehi and M. Kavianty, Adiabatic reverse combustion in a packed bed, *Comb Flame*, 99, pp. 1-17, 1994.

[24] S. Bandyopadhyay, R. Chowdhury, G.K. Biswas, Transient behavior of a coconut shell pyrolyzer: A Mathematical Analysis, *Ind Eng Chem Res*, 35, pp. 3347-55, 1996.

[25] B. Peters, E. Schröder, Bruch C. Measurements and particle resolved modelling of the thermo- and fluid dynamics of a packed bed, *J. Anal. Appl. Pyrolysis*, 70, pp. 211-31, 2003.

[26] C. Di Blasi, C. Branca, B. Teislev, Development of a novel reactor for the oxidative degradation of straw, *Biores Technol,* 91, pp. 263–71, 2004.

[27] K. Tanoue, T. Suetomi, T. Nishimura, M. Taniguchi, K. Sasauchi, Thermal conduction and gas generation undergoing pyrolysis in the packed bed of woody biomass, *J. Japan Inst. Energ,* 91, pp. 976-84, 2012, (in Japanese).

[28] C. Di Blasi, G. Russo, Modeling of Transport Phenomena and Kinetics of Biomass Pyrolysis. In: Bridgwater A.V. (eds) *Advances in Thermochemical Biomass Conversion*, Dordrecht: Springer, pp. 906-921, 1993.

[29] R.B. Bird, W.W. Stewart, E.N. Lightfoot. *Transport Phenomena*, Int Student Edition, New York: Wiley, 1960.

[30] T. Koya, D. Kunii, Measurement of thermal conductivities of solid particles in packed beds. Kagaku Kogaku, 35, pp. 912-16, 1971 (in Japanese).

[31] R.H. Perry, C.H. Chilton, *Chemical Engineer's Handbook*. 5th Edition (Int student ed), Tokyo: McGraw-Hill Kogakusya Ltd, 1973.

[32] H. Wenzl, *The chemical technology of wood*. New York: Academic Press Inc.,1970.

[33] R.H. Perry and D. Green, *Perry's chemical engineers' handbook*, 6th Edition, New York: McGraw-Hill, 1984.

[34] M.G. Gronli, M.C. Melaaen, Mathematical model for wood pyrolysis – comparison of experimental measurements with model predictions, *Energy& Fuels*, 14 (4), pp. 791–800, 2000.

[35] https://www.isolite.co.jp/en/products/taika/b_insulation/

[36] C.K. Lee, R.F. Chaiken, J.M. Singer. Charring pyrolysis of wood in fires by laser simulation, *Proc. of the Combust Inst*, pp. 1459–70,1976.